







Article

Investigations on Tailored Forming of AISI 52100 as Rolling Bearing Raceway

Timm Coors ^{1,*}, Maximilian Mildebrath ², Christoph Büdenbender ³, Felix Saure ¹, Mohamad Yusuf Faqiri ², Christoph Kahra ², Vannila Prasanthan ⁴, Anna Chugreeva ³, Tim Matthias ³, Laura Budde ⁵, Florian Pape ¹, Florian Nürnberger ², Thomas Hassel ², Jörg Hermsdorf ⁵, Ludger Overmeyer ⁵, Bernd Breidenstein ⁴, Berend Denkena ⁴, Bernd-Arno Behrens ³, Hans Jürgen Maier ² and Gerhard Poll ¹

¹ Institut für Maschinenkonstruktion und Tribologie (Machine Design and Tribology), Leibniz University Hannover, An der Universität 1, 30823 Garbsen, Germany; saure@imkt.uni-hannover.de (F.S.); pape@imkt.uni-hannover.de (F.P.); poll@imkt.uni-hannover.de (G.P.)

² Institut für Werkstoffkunde (Materials Science), Leibniz University Hannover, An der Universität 2, 30823 Garbsen, Germany; mildebrath@iw.uni-hannover.de (M.M.); faqiri@iw.uni-hannover.de (M.Y.F.); kahra@iw.uni-hannover.de (C.K.); nuernberger@iw.uni-hannover.de (F.N.); hassel@iw.uni-hannover.de (T.H.); maier@iw.uni-hannover.de (H.J.M.)

³ Institut für Umformtechnik und Umformmaschinen (Forming Technology and Machines), Leibniz University Hannover, An der Universität 2, 30823 Garbsen, Germany; buedenbender@ifum.uni-hannover.de (C.B.); chugreeva@ifum.uni-hannover.de (A.C.); tmatthias@ifum.uni-hannover.de (T.M.); behrens@ifum.uni-hannover.de (B.-A.B.)

⁴ Institut für Fertigungstechnik und Werkzeugmaschinen (Production Engineering and Machine Tools), Leibniz University Hannover, An der Universität 2, 30823 Garbsen, Germany; prasanthan@ifw.uni-hannover.de (V.P.); breidenstein@ifw.uni-hannover.de (B.B.); denkena@ifw.uni-hannover.de (B.D.)

⁵ Laser Zentrum Hannover e.V., Hollerithallee 8, 30419 Hannover, Germany; l.budde@lzh.de (L.B.); j.hermsdorf@lzh.de (J.H.); ludger.overmeyer@ita.uni-hannover.de (L.O.)

* Correspondence: coors@imkt.uni-hannover.de; Tel.: +49-511-762-5552

Received: 31 August 2020; Accepted: 10 October 2020; Published: 13 October 2020



Abstract: Hybrid cylindrical roller thrust bearing washers of type 81212 were manufactured by tailored forming. An AISI 1022M base material, featuring a sufficient strength for structural loads, was clad with the bearing steel AISI 52100 by plasma transferred arc welding (PTA). Though AISI 52100 is generally regarded as non-weldable, it could be applied as a cladding material by adjusting PTA parameters. The clad parts were investigated after each individual process step and subsequently tested under rolling contact load. Welding defects that could not be completely eliminated by the subsequent hot forming were characterized by means of scanning acoustic microscopy and micrographs. Below the surface, pores with a typical size of ten μm were found to a depth of about 0.45 mm. In the material transition zone and between individual weld seams, larger voids were observed. Grinding of the surface after heat treatment caused compressive residual stresses near the surface with a relatively small depth. Fatigue tests were carried out on an FE8 test rig. Eighty-two percent of the calculated rating life for conventional bearings was achieved. A high failure slope of the Weibull regression was determined. A relationship between the weld defects and the fatigue behavior is likely.

Keywords: tailored forming; hybrid bearing; AISI 52100; plasma transferred arc welding; residual stress; scanning acoustic microscopy; bearing fatigue life

1. Introduction

In many technical applications, functional part regions of components experience a significantly higher load than basic structural regions. This occurs, for example, due to rolling contacts, like rolling bearings or gears. The material at and just below the surface, such as the raceway of the bearing, can experience very high stresses of over 3000 MPa and exceed 10^6 load cycles. In order to achieve a long lifetime, the material needs to be of a high quality, strength, and hardness. Mounting components such as shafts or less stressed regions in gear wheels like the connecting structure between the hub and teeth are subjected to a much lower load. Depending on the application, a base material with reduced strength or a lighter material may be sufficient or even advantageous.

Especially in large size bearings, the material costs for high purity steels that are mostly free of tramp elements are very high. Thus, a compromise between costs and benefit has to be made. The localized application of a layer of a high-performance material in the highly loaded area improves the mechanical properties where these are required. A base material, which is located in the less highly loaded region, can save costs and can fulfill other functions regarding, e.g., weight reduction or a modified ductility. These multi-material components can be adapted to thermal, environmental, and mechanical stresses depending on the application.

2. State-of-the-Art

The Collaborative Research Center (SFB) 1153 tailored forming aims to develop and optimize a novel process chain for the manufacturing of hybrid solid components. This is done by thermomechanically joining semi-finished products and subsequent forming to produce components with locally adapted properties. By combining different materials within one component, it is possible to reduce the component weight by the local use of lightweight materials or to reduce cost by combining low-cost base materials with high-quality alloys at certain functional surfaces. Among others, the mechanical properties of a hybrid cylindrical roller thrust bearing are of interest. Thus, the low-alloy steel AISI 1022M (material number 1.0460) was used as base material, clad by the steel AISI 52100 (1.3505) and produced using the tailored forming technology to manufacture hybrid bearing washers. This process chain is depicted schematically in Figure 1. In the first step, the high strength steel was cladded onto the base materials using plasma transferred arc powder deposition (PTA) welding (Figure 1a). Subsequently, the hybrid workpiece was formed into the semi-finished product with a near net-shaped contour by means of forging (Figure 1b). This thermomechanical treatment improved the quality of the interface zones, as shown for deposition welded workpieces in [1,2]. In the following, a heat treatment by means of quenching and tempering, as well as a subsequent machining (Figure 1c), were carried out to produce the axial bearings as depicted in Figure 1d. In the load direction, the two hybrid discs on which the rolling element was running featured a material transition, with the high strength material serving as the raceway.

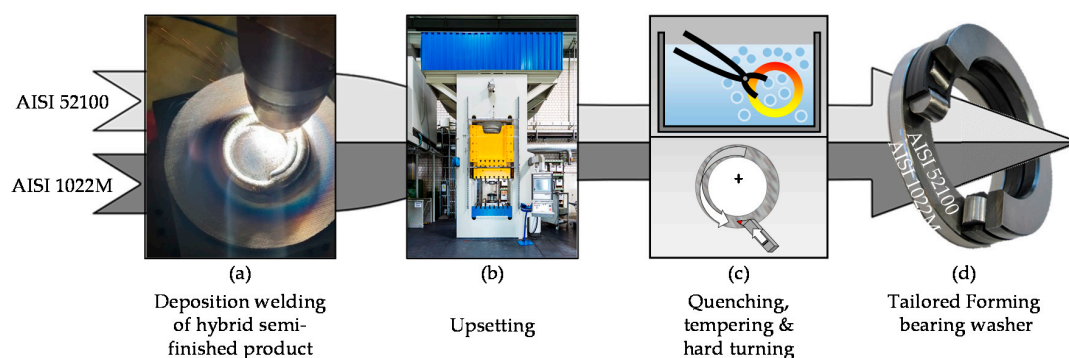


Figure 1. Process chain for manufacturing a hybrid cylindrical roller thrust bearing washer by tailored forming: (a) plasma-transferred arc deposition welding; (b) upsetting; (c) heat treatment by quenching, tempering, and subsequent mechanical processing; (d) bearing assembly for analysis in a test bench.

In the following, the term “hybrid bearing” is used for multi-material bearing components manufactured by means of tailored forming. Here, the application of two different materials with a material transition in the load direction is characteristic. In contrast, the term “hybrid” in the context of rolling bearings is usually employed for bearings in which different materials are combined for the bearing rings and rolling elements [3]. Nitrided rolling bearing steel is often used for the bearing rings and a high-strength ceramic, such as silicon nitride, for the rolling elements [4]. These bearings are suited for high performance applications and are complex regarding their proper evaluation [5].

Regarding iron-based cladded components and their fatigue behavior under complex loads due to rolling contacts, few previous works exist. Koehler et al. welded ASTM F75 powder (American Society for Testing and Materials standard for cobalt-28 chromium-6 molybdenum alloy; material number 2.4979) via deposition welding on AISI 4140 (American Iron and Steel Institute standard; 1.7225) and detected a reduced fatigue strength in 4-point bending tests compared to the mono-material, which could be explained by tensile residual stresses caused by the cladding process [6]. In further research by Koehler et al., fatigue tests were carried out on crankshafts of the same material combination repaired by deposition welding [7]. The specimen showed a reduced tensile strength and yield stress compared to newly manufactured crankshafts, resulting in a reduced fatigue life. Alam et al. cladded ASTM F75 on ASTM A572 (1.0045) and observed pores on the surfaces of cylindrical and square bars [8]. It was found that surface cracks were initiated due to these pores, with a negative effect on service life. Pores or defects below the surface were not investigated. In Chew et al., a cladding of 1 mm of ASTM F75 was applied to AISI 4340 (1.6511). Cross-section examination of the specimen showed that no macro defects such as pores, lack of fusion, or cracking appeared [9]. By further surface grinding processes of the specimen, a maximum fatigue life of 95% compared to the monolithic substrate could be achieved. At the location of direction change in the course of the welding track, early fatigue cracks were initiated due to the higher heat input and the local microstructure evolution. The positive influence of compressive residual stresses on the fatigue life of radial bearings made of AISI 52100 was investigated in [10]. In contrast to the aforementioned, tests were carried out on real components under a high Hertzian contact pressure of 2.5 GPa. By hard-turning and subsequent deep rolling, an improvement in service life was achieved in comparison to ground hybrid bearings.

Blohm et al. [1] used a subsequent forming process for shafts from AISI 1022M cladded with AISI 5140 (1.7035) by PTA welding. Due to this forming process, a defect-free interface zone could be obtained. Using the example of a hot-formed specimen manufactured by welding, Mildebrath et al. [2,11] demonstrated that the cladding completely recrystallized during the subsequent forming process and that disadvantageous microstructures present after welding were transformed. Behrens et al. [12] researched hybrid forging billets that were welded out of alloy steel AISI 5140 and carbon steel AISI 1022M. They employed a test matrix that utilized the variations of process parameters to influence the geometry and microstructure of the materials' joining zone. Pape et al. [13] investigated the manufacturability of multimaterial components by combining the high-alloy steel AISI HNV3 (1.4718) with the base substrate of ASTM A283 (1.0038) in a single component. The materials were joined by laser metal deposition by wire according to the stressed zones of the component and examined. The aim was to ensure an efficient use of resources. Behrens et al. [14] welded bearing washers of AISI 1022M with the alloyed steel AISI 5140. They researched the grain refinement depending on the degree of forming and investigated the wear resistance of the specimen. Stanford and Jain [15] found that pores in the loaded material areas had the greatest influence on the service life of the components if they had not been closed or reduced in size by a subsequent forming process. In particular, they emphasized the positive influence of the forming process on fatigue life.

3. Aim and Research Objectives

As has been shown in the State-of-the-Art Processes section, the deposition welding of a low-alloyed steel can result in a reduction in its fatigue strength. The build-up welded surfaces of low-alloyed steels do not yet have sufficient fatigue resistance to rolling bearing loads. No references are known for

the welding and subsequent forming of rolling bearing steel. The aim of this study was therefore to develop a process route for the application of rolling bearing steel by means of tailored forming and to investigate the mechanical properties of the components produced in this way. For this purpose, the following questions have to be answered:

1. Which welding parameters are necessary to functionalize bearing steel that is normally declared as not weldable?
2. How do the downstream processes need to be adjusted in order to achieve a high component quality for use as rolling bearings raceways?
3. What is the microstructure of the material compound after the different manufacturing steps?
4. Were the relevant component properties for use as a rolling bearing component achieved?
5. What are the relevant mechanisms that govern the fatigue behavior?
6. What damage patterns occur when used as a rolling bearing raceway?

4. Materials and Methods

In this study, classical bearing steel was welded on a base material by means of plasma-powder-transferred arc welding (PTA) and later used as bearing raceway of a cylindrical roller thrust bearing type 81212, see Figure 2. A washer with an outer diameter of 95 mm was produced, see Figure 2a. The washers' thickness was 7.5 mm. It had a material transition in axial direction (Figure 2b), which was the direction of loading. The base material of the washer consisted of the unalloyed and heat-resistant weldable steel AISI 1022M, which is mainly used in valve construction. The cladding material for the PTA consisted of the rolling bearing steel AISI 52100, which had a CEV > 1 and was considered to be non-weldable [16]. In order to weld the material in spite of this, the material was atomized to utilize it for PTA. The material AISI 52100 has a high wear resistance and toughness, which is why components such as rolling bearings are made of it. The chemical compositions of the materials are shown in Table 1. The chemical compositions were measured with a spark analyzer LMX07 (Spectro Analytical Instruments GmbH, Kleve, Germany).

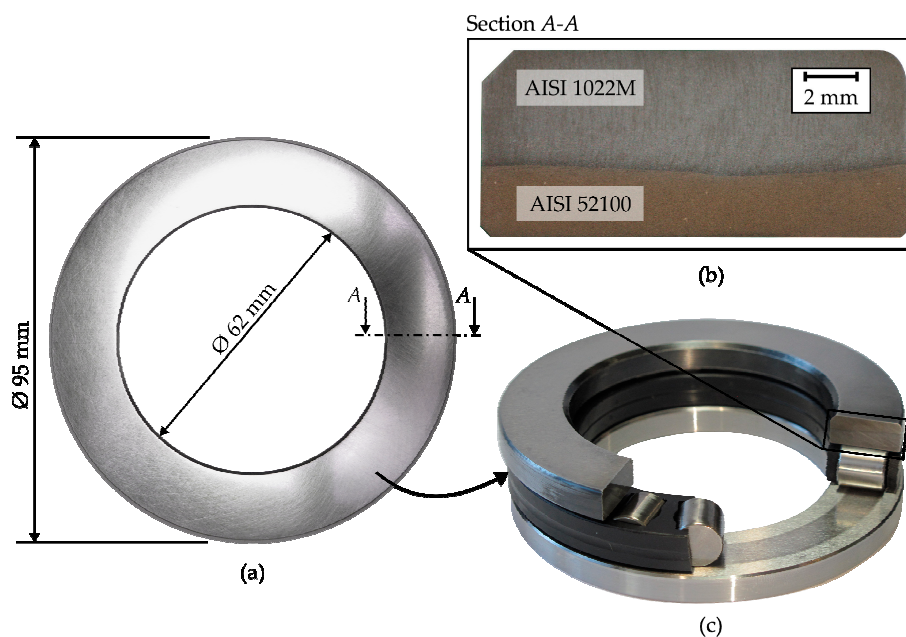


Figure 2. Tailored forming bearing: (a) finished specimen as roller bearing raceway; (b) sectional view; (c) cylindrical roller thrust bearing type 81212.

Table 1. Chemical composition of AISI 1022M and AISI 52100 determined by optical emission spectrometry in wt.%.

| AISI | C | Si | Mn | P | S | Cr |
|--------|------|------|------|------|-------|------|
| 1022 M | 0.22 | 0.29 | 0.84 | 0.01 | 0.001 | 0.04 |
| 52100 | 0.97 | 0.25 | 0.31 | 0.01 | 0.004 | 1.38 |

After PTA welding, the component was formed to improve the material properties. By means of detailed analytical methods, the processes necessary for production were investigated step by step. The components that were produced, as described in Figure 1, later served as rolling bearings and will be characterized in the following with regard to their material properties. Subsequently, fatigue tests were carried out on a rolling bearing test rig, which served as a baseline for further investigations. The roller and cage assembly was taken from conventional bearings, in order to assemble a cylindrical roller thrust bearing consisting of two discs, see Figure 2c.

4.1. Plasma Transferred Arc Deposition Welding

PTA is a thermal process for applying wear and corrosion resistant layers on surfaces of metallic materials. During the PTA welding process, a tungsten electrode created a plasma arc with high energy density, which melted the surface of the base material. At the same time, the cladding material was inserted into the arc by a powder stream and was molten. During solidification, a substance-to-substance bond between the cladding and base material was created. The welding process was shielded by argon gas. The advantages of this process were a low dilution rate, a small heat affected zone, and deposition rates up to 10 kg/h. Further benefits were a high degree of automation and reproducibility [17].

The welding process was carried out on a six-axis REIS RV industrial robot (KUKA AG, Augsburg, Germany), where two additional axes were realized by a turn and tilt table. The welding torch was a Kennametal Stellite HPM 302 (Kennametal Stellite, Pittsburgh, PA, USA), which was water-cooled. The equipment is shown in Figure 3a. To obtain the optimum grain size with a diameter of a minimum 63 μm to maximum 200 μm , the powder was filtered with sieving units (Retsch, Haan, Germany). This corresponds to the current industrial standard for additional materials in powder form that are used for PTA welding [18]. Powders with the standard grain size were used because of a regular melting behavior in the arc as well as a good transportability in the gas flow of the transport gas. Prior to the welding process, the surface of the discs was cleaned with acetone (E-Coll, Wuppertal, Germany). The substrate was at room temperature at the start of welding and was not preheated. Welding without preheating normally makes a welding process more difficult, especially when high carbon equivalent steels are processed. However, by choosing a slow welding speed of 0.12 m/min, the resulting high heat input enabled the discs to be heated up to suitable joining temperatures in a short time by the welding process itself. This improved the weldability of the steel alloys used. The disc was placed on the additional axis, which was aligned parallel to the ground. Due to the spiral-shaped seam geometry (Figure 3a), the beginning and the end of the seam were not located in the area where the rolling contact will later take place. Therefore, any defects that occur in the beginning or the end of the weld, e.g., because of too low or too high temperatures, were not relevant for the later function of the components. During the welding process, the torch oscillated with a frequency of 2.0 Hz and amplitude of 4 mm at an angle of 90° to the welding direction. The oscillation increased the dynamics of the weld pool and allowed the degassing of the melt, preventing pores. The welding process took about 10 min and 30 s, whereby the disc heated up to 650 °C. To keep the dilution between the base material and cladding metal nearly constant, the welding current was dynamically adapted during the welding process (see Figure 3b). Starting with a current of 180 A, the current was gradually reduced to 130 A. A suitable current curve was empirically determined in preliminary tests by temperature measurements accompanying the welding process. A short working distance of 10 mm was selected. This allows a very precise control of the seam geometry. This was set with a seam-overlap of 1.5 mm.

Due to the short working distance, the plasma gas was set as low as possible at 1.5 min^{-1} to avoid spattering of the melt pool. The remaining gas values for transport and protective gas correspond to standard values. An overview of the general welding parameters is given in Table 2.

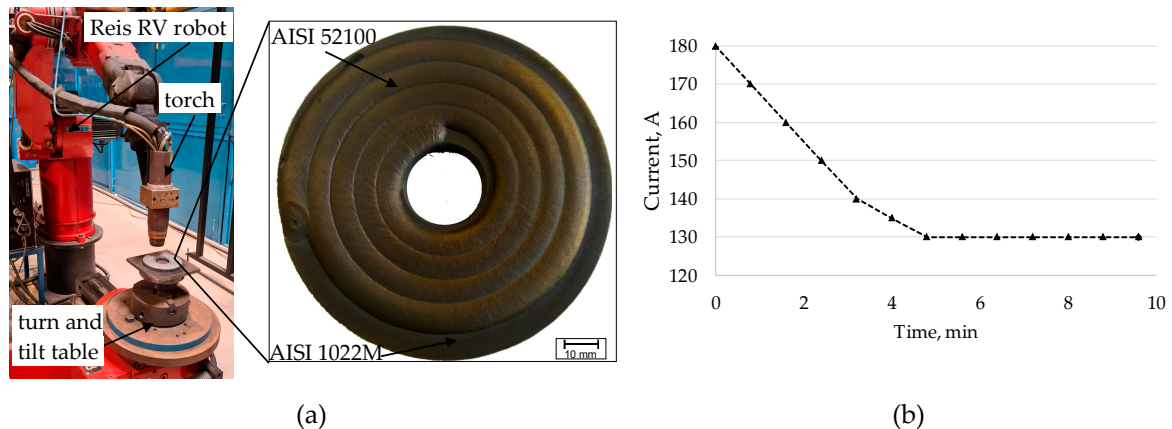


Figure 3. (a) Experimental setup of the welding process; (b) adjustment of current intensity.

Table 2. Welding parameters.

| Parameter | Value | Parameter | Value |
|----------------------------|------------|-----------------|-------------|
| Shielding gas flow (argon) | 10 L/min | Current | 180–130 A |
| Plasma gas flow (argon) | 1.5 L/min | Voltage | 25–27 V |
| Transport gas flow (argon) | 6 L/min | Powder material | AISI 52100 |
| Welding velocity | 0.12 m/min | Particle size | 0.06–0.2 mm |
| Working distance | 10 mm | Deposition rate | 0.9 kg/h |

4.2. Upsetting

After deposition welding, the hybrid bearing washers were formed in a single-stage upsetting process. The application of forming allowed to improve the welded microstructure by thermomechanical treatment and to close the pores in the cladding layer [19]. The upsetting was performed on a hydraulic press (SPS Schirmer-Plate Siempelkamp GmbH, Krefeld, Germany) with a maximum capacity of 12,500 kN, as depicted in Figure 4a. The required forging temperature of 1050°C was achieved by heating in a chamber furnace (Nabertherm, Lilienthal, Germany) in an inert gas atmosphere (Figure 4b) in order to prevent the surface decarburization and oxidation of the weld material. After the individual workpieces were put in the shielding gas container, the air was displaced by argon within a timeframe of 15 min. Then, the container was placed in the furnace until the workpieces were heated up within a timeframe of 20 min. Subsequently, the hot preforms for bearing washers were manually transferred to the forming tool and formed by upsetting from 15 mm to 9 mm. After forging, the bearing washers were cooled in air. A bearing washer after forming is shown in Figure 4c. The main parameters of the forging are summarized in Table 3.

Table 3. Parameters of upsetting process.

| Parameter | Value |
|-----------------------|----------------------|
| Forming temperature | 1050°C |
| Furnace shielding gas | argon |
| Forging force | 1700 kN |
| Height reduction | 35% |
| Final height | 9 mm |

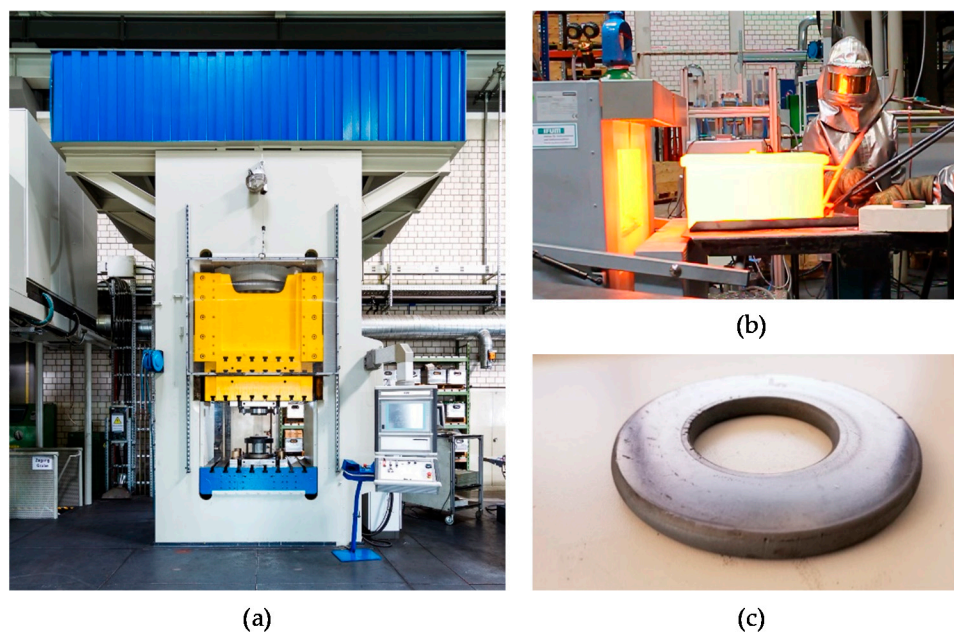


Figure 4. Forming setup: (a) hydraulic press; (b) removal of the shielding gas container from the furnace after heating of the workpieces; (c) forged bearing washer.

The macrographs depicted in Figure 5 show the effect of the die forging on the material distribution for the example of a bearing washer preform that is welded with a single seam. Both samples were prepared from the same workpiece, which was separated in two parts. One of them was subsequently formed; the second one remained without any further treatment. The mentioned parts were metallographically investigated at several positions. The representative results of this examination are illustratively demonstrated in Figure 5. After upsetting, the weld material was pressed into the substrate. A flattening of the cladding surface took place as a result of the forming process. After the deposition welding, some pores marked with red circles in Figure 5a were macroscopically observed close to the joining zone area. After forging, no pores at the investigated positions could be seen at the macroscopic scale (Figure 5b). A quantitative comparison of the porosity before and after forging was, however, not possible because the cross-sections of cladmed and forged parts were not extracted from the same position. Forming is not only able to close pores; non-metallic inclusions are also pressed further into the depth of the surface, and thus out of the intended loaded functional area. This is also a desirable effect, as pores or defects directly below the surface are the most critical ones [6].

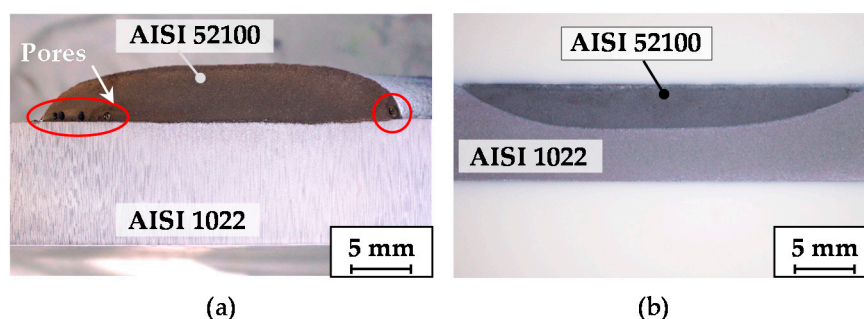


Figure 5. (a) Section view of the cladmed workpiece welded with a single seam and (b) of a near-net-shaped bearing washers after forging (etched with nitric acid solution).

4.3. Heat Treatment

To adjust the required strength and hardness of the bearing washers, a heat treatment in terms of quenching and tempering was carried out after the machining. For this purpose, the bearing washers

were placed in a self-designed hardening box with neutral annealing coal. The box was equipped with a thermocouple and preheated to 850 °C in an electrically heated chamber furnace. The bearing washers were austenitized at this temperature for 45 min (heating + holding time). In addition to the neutral annealing coal, argon was used to further prevent decarburization of the parts. To avoid stress cracks, quenching was carried out in an oil bath at room temperature. Subsequently, the bearing washers were tempered at 150 °C for 1 h to reduce brittleness and internal stresses, and achieve a target hardness of 60 according to Rockwell C (HRC) (measured on industrial bearing raceway).

4.4. Machining

After the upsetting process in the process chain of manufacturing hybrid bearing washers, water jet cutting was employed to produce the annular geometry and the component was pre-machined to tolerance with a 1-mm off-cut. After the subsequent heat treatment, the final geometry was obtained by a grinding process (Figure 6). This was conducted on a grinding machine with computerized numerical control (CNC) of type Blohm Orbit 48 (Blohm Jung GmbH, Hamburg, Germany). A surface grinding wheel type 517A 54/11 G7H 2020 V341A (Butzbacher Schleifmittel-Werke GmbH, Butzbach, Germany) was used here for the finishing operation step. In order to fulfill the surface quality requirements, a cutting speed of $v_c = 25$ m/s, a feed of $f = 200$ mm, and a depth of cut of $a_e = 100$ µm were applied.

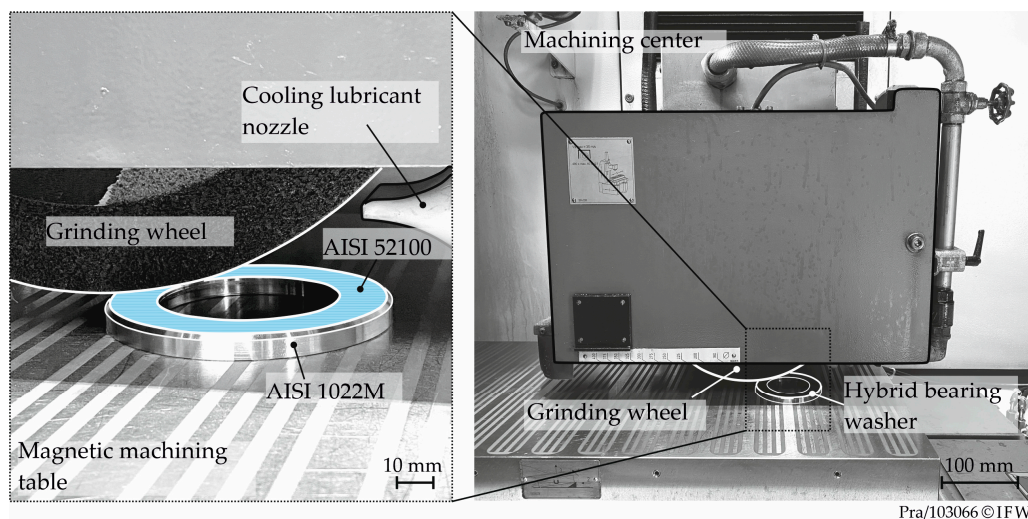


Figure 6. Machining setup in the CNC grinding machine.

4.5. Analytical Methods

4.5.1. Metallographic Investigations and Hardness Measurements

For microstructural characterization of the interface zone, cross-sections were extracted from the bearing washers in a radial direction. Metallographic investigations were carried out after deposition welding, hot forming, and heat treatment in order to examine the microstructural evolution. The samples were prepared metallographically by grinding, polishing, and subsequently etched with the reagent Beraha I or 2% nitric acid solution (CRIDA Chemie, Wenden, Germany). To investigate the hardness distribution across the joining zone, hardness measurements were carried out after each process step. Hardness testing on a ATM Q10A+ (ATM Qness GmbH, Mammelzen, Germany) according to Vickers HV 0.5 standard was used for this purpose [20]. Hardness profiles were measured from the AISI 52100 surface of the bearing disc in the AISI 1022M base material. To compare the surface hardness of the tailored forming bearing washer with an industrial bearing washer, hardness measurements were carried out after the bearing washer was manufactured. The Rockwell HRC hardness test according to DIN EN ISO 6508 was used for this purpose [21].

4.5.2. Residual Stress Measurements

Due to different thermal expansion coefficients of the materials, delayed cooling of the subsurface and core, as well as local structural transformations limited to the surface layer; residual stresses were caused after forging and the heat treatment process, which were modified by subsequent machining of the hybrid component [22,23]. Residual stresses have a significant influence on the operating behavior and therefore the lifetime of a component. The fatigue life of a cyclically loaded component is reduced by high internal tensile residual stresses because they lead to failure of the component by crack formation and propagation. Compressive residual stresses, however, can increase the component's service life by reducing crack initiation and propagation [24–26]. For this reason, it was necessary to analyze the residual stress condition of a component before the tribological investigations.

The residual stresses were determined radiographically using the $\sin^2\psi$ -method [27,28]. A Seifert XRD 3003TT two circle X-ray diffractometer (Röntgenwerk Rich. Seifert & Co., Ahrensburg, Germany), equipped with a Cr tube and a spatially resolved detector, was used for this purpose. The point focus measuring spot was delimited with a 2-mm point collimator. The ω -axis of the diffractometer served as tilting axis ψ . For measurement on the martensitic phase, the tilt range of ψ varied from -45° to $+45^\circ$ with a total of nine tilt positions. To determine the net plane spacing d_{211} of the α -iron, the intensity was recorded over 2θ in the range between 144.0° and 164.8° with a step size of 0.2° . The measurement time per step was 36 s. The maximum information depth of the X-radiation was $\tau_{max} = 5.5 \mu\text{m}$. For measurements at a greater distance from the surface, material was successively removed by electrolytic polishing. For the X-ray elasticity constants s_1 , $\frac{1}{2}s_2$, and the reference values for the unstressed material, the values of the pure α -iron grid were assumed [29]. The evaluation of the residual stress measurements was carried out with the RayfleX software (Version 2.501, Röntgenwerk Rich. Seifert & Co., Ahrensburg, Germany) from General Electric. After data reduction, the position of the diffraction reflections was determined using the parabolic fit method. The data reduction was carried out according to the following procedure: smoothing according to the Savitzky and Golay algorithm, left-sided background correction, intensity corrections, and a parabola fit with a threshold value of 70% of the maximum intensity. The measuring accuracy of the X-ray diffractometer specified by the manufacturer for flat sample geometries was $\sigma = \pm 10 \text{ MPa}$.

4.5.3. Non-Destructive Examination

The nanomechanical properties of the bearing washers were investigated before forming and after finishing. The aim of the tests was to determine the frictional and mechanical surface properties of the hybrid bearing washer. Nano-scratch tests were carried out with a Hysitron TriboIndenter TI950 (Bruker Corporation, Billerica, MA, USA). A cono-spherical diamond tip with a radius of 300 nm was used. The measured values were used to determine the elastic and plastic deformation behavior and the penetration-dependent friction coefficient μ during ploughing. The measuring tip traveled along the specimen surface with linearly increasing normal load and constant speed. It was moved over the sample with electrostatic force resulting in a tangential force. As the normal force increased during ploughing (Scratch test), the tangential force also increased. By the change in capacitance, the system detected the tangential force in dependence on the normal force and the depth displacement. According to these data, the coefficient of friction μ based on Coulomb friction was calculated. In the tests, a maximum load of the tip of 1 mN was used. The surface profile was analyzed before and after the scratch test using Scanning Probe Microscopy (SPM). The travel length of the tip was about 8 μm . The test was divided in three steps. First, the initial surface profile was scanned by the tip under a low load on the scratch path (prescan). Next, the scratch was performed on the same route with a load magnitude of 1 mN (scratch). To determine the resulting plastic deformation, the scratch route was scanned again with a low force magnitude (postscan). By analyzing the prescan, scratch, and postscan profile, it was possible to record the elastic and plastic deformation by calculating the different penetration depths. The plastic behavior was calculated based on five measurements and the standard deviation was determined.

Non-destructive testing using scanning acoustic microscopy (SAM) with a modified PVA TePla SAM 301 system (PVA TePla, Wetzlar, Germany) was used to examine the components for sub-surface damages after production and after fatigue testing. Here, the scanner-mounted transducer generates a pulse into the sample in the ultrasonic frequency range. The sound pulse is partially or completely scattered and reflected by inhomogeneities in the material, which are then measured (pulse-echo method). Distilled water served as a coupling medium between transducer and samples. Penetrating oil was used as a corrosion inhibitor. The surface roughness of the raceway was measured tactilely with a Mahr Perthometer PCV (Mahr-Gruppe, Göttingen, Germany). The measurement was carried out in radial and in circumferential direction of the disc at five points each.

4.5.4. Bearing Fatigue Testing

In order to investigate the performance of the hybrid bearing washers, bearing fatigue tests were carried out on a self-designed FE8 test rig according to DIN 51819 [30]. The test rig was originally used for the dynamic-mechanical testing of automotive and industrial lubricants. In the FE8 test head, two cylindrical roller thrust bearings of type 81212 were mounted on a single shaft, see Figure 7. Each bearing consisted of a bearing washer that was fixed in the housing and a washer that rotated with the shaft, as well as the rolling elements and cage. Only one tailored forming housing washer was used for bearing fatigue testing, while the other washers were taken from conventional 81212 bearings. For these investigations, 19 rolling elements mounted in a fiberglass-reinforced polyamide cage were used. The conventional rolling elements and washers were made from martensitic through-hardened AISI 52100. The force was applied by a disc spring assembly in axial direction and measured by a HBM C2 load cell (Hottinger Baldwin Messtechnik GmbH, Darmstadt, Germany) during mounting. For an initial functional test, the test parameters from previous tests with other cladding materials were applied [13,14]. Here, the axial load was 40 kN. Due to very high run times, the load was increased to 60 kN for the subsequent fatigue tests. The test parameters are specified in chapter 0. A circulating lubrication system with a filtration quotient of $\beta_{10} = 200$ according to ISO 16889 supplied each bearing with lubricant at a rate of 0.1 L/min via the housing side [31]. The lubricant used was a commercial gear oil based on synthetic polyalphaolefins with a viscosity grade of ISO VG 68 (Fuchs Petrolub SE, Mannheim, Germany). The oil contained, among other additives, extreme-pressure and anti-wear additives. Failure by spalling on the washer's raceway was manifested as a sudden increase in vibration, which was used as a termination criterion. A threshold of 150% of the steady state signal had to be exceeded for the test to shut down. The tests were carried out using the sudden death method.

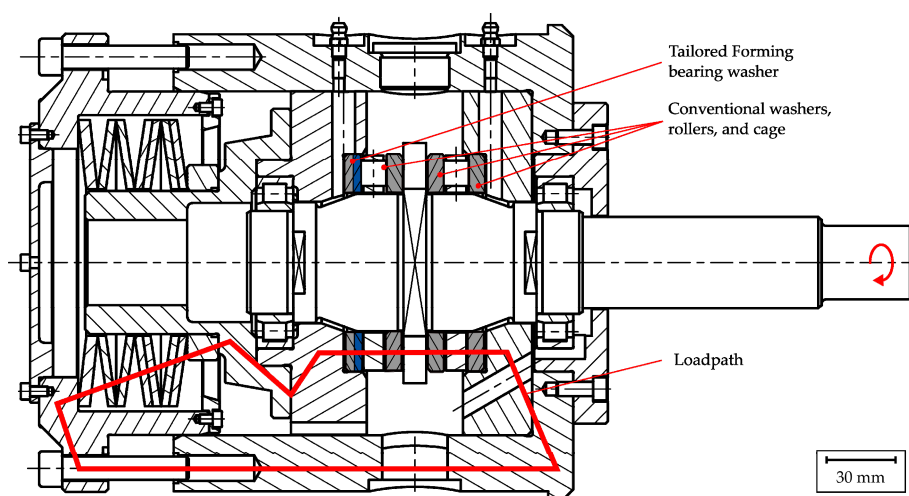


Figure 7. FE8 test head with type 81212 cylindrical roller thrust bearing.

5. Results and Discussion

5.1. Microstructure Evolution during Processing

The micrographs, showing the transition of the cladding layer into the base material, are illustrated in Figure 8. Figure 8a shows the microstructure after deposition welding. The base material AISI 1022M has a ferritic-pearlitic microstructure with large grains. Close to the joining zone, needle-shaped Widmanstätten ferrite could be observed. The microstructure of the cladding material was mainly pearlitic. Figure 8b shows the microstructure of the hot-formed and air-cooled bearing washers. Here, the base material also consisted of a ferritic-pearlitic microstructure and the clad material of a mainly pearlitic microstructure. However, the microstructure was more homogeneous and fine-grained compared to the welded state due to hot forming-induced recrystallization. The micrographs taken after hardening, i.e., quenching and tempering, are shown in Figure 8c. The microstructure of the cladding material was completely transformed into martensite during hardening by quenching, featuring a needle-shaped morphology. Martensite was also formed close to the interface zone in the base material, though the remainder of the base material was ferritic-pearlitic. The results from the hardness measurements (Figure 9) were in accordance with the metallographic investigations. The hardness profiles of the bearing washers after deposition welding and after forming were very similar, since the components were cooled in air after the respective process step and thus have not been subjected to any specific heat treatment to increase the hardness. After the targeted heat treatment by quenching and tempering of the bearing washers, a hardness of 880 HV0.5 was determined in the cladding layer and of 250 HV0.5 in the base material. The base material remained ductile after hardening, while the cladding featured high hardness values as desired to withstand the rolling contact loads. The lower hardness in the base material resulted from the low carbon content of the steel AISI 1022M. The hardness was examined again on the cutting surface after the process steps of deposition welding, forming, and hardening (see Figure 9). The results show that the mean hardness after deposition welding and the forming process did not differ in the cladding material. It can be observed that there was a gradient from the cladding material to the base material. The hardness in the cladding material increased again after targeted heat treatment of the bearing washer. While an almost defect-free material transition between the base material and the cladding material was achieved by upsetting, the subsequent heat treatment allowed to achieve hardness values for the tailored forming bearings that are similar to those of the industrial bearings, which were also measured at 60 HRC.

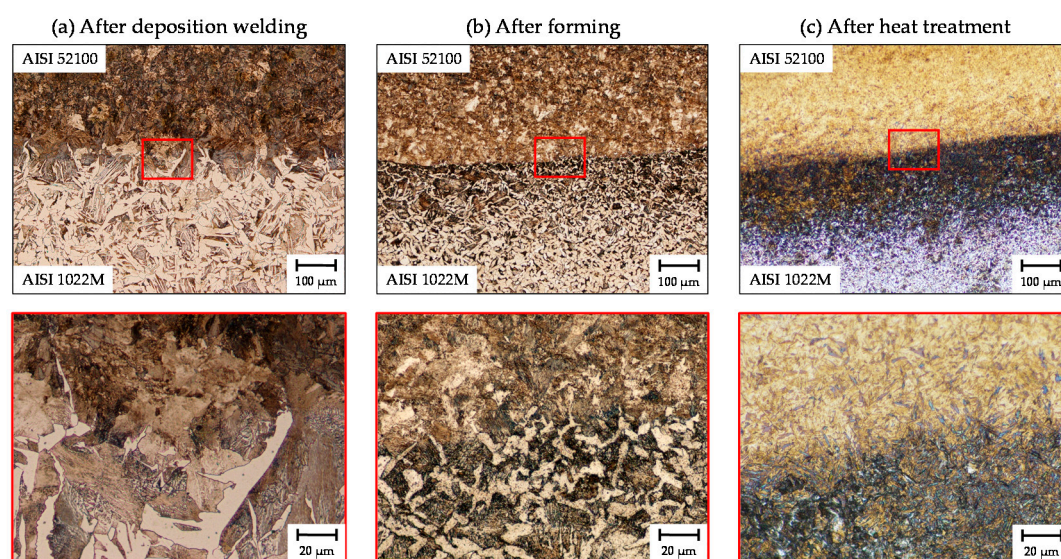


Figure 8. Micrographs of the joining zone: (a) After deposition welding; (b) after forming; (c) after a quenching and tempering heat treatment; (a,c) etched with 2% nitric acid solution; (b) etched with Beraha I reagent.

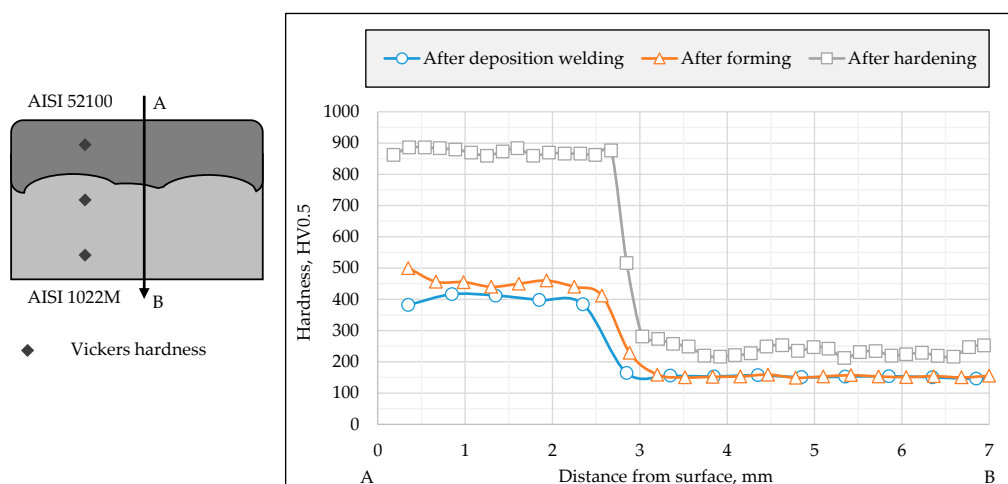


Figure 9. Hardness profiles of the hybrid bearing washers.

The chemical composition measured by spark spectroscopy showed that the carbon content was slightly below the values specified for AISI 52100 (0.87% instead of at least 0.93%, see EN 10132-4), c.f. Table 1. The reduced carbon content is attributed to the welding process, as the elemental content was slightly reduced due to the material dilution between the base material and the cladding material.

5.2. Residual Stress State

In Figure 10, the residual stress depth profiles and the corresponding peak halfwidths (full width at half maximum, abbreviated as FWHM) depth profiles of a machined hybrid axial-bearing washer are presented. The residual stress depth curves show that in both directions (circumference $\varphi = 0^\circ$ of the bearing washers as well as radially $\varphi = 90^\circ$) maximum compressive residual stresses occurred near the surface of the hybrid component. With increasing surface distance, a very abrupt shift in the direction of tensile residual stresses was noticeable. A significant difference in the residual stress profile depending on the measuring direction was not visible in the surface-near area. Only from a surface depth of approx. 50 μm did deviations occur in the residual stress profiles between radial and circumferential direction.

Taking a closer look at the associated FWHM in connection with the residual stress measurement, it is clear that a relatively similar course of the profiles can be seen here as well. The differences between the two measuring directions are not significant. It is apparent that the FWHM at the surface was high, then decreased with further increasing surface distance and reached a minimum at approx. 4 μm depth. With further increasing surface distance, the FWHM value increased again and reached the value of the basic structure. The area that was influenced by the grinding process was only minimal and lies approximately in the range between 0 and 50 μm . The FWHM was an indication of the plastic deformation and thus of the hardening state of the surface as a result of increased or decreased dislocation density. There was a proportional relationship between plastic deformation and FWHM, which means that, with increasing plastic deformation, the FWHM would also increase. The grinding process caused a softening of the material in the surface-near area. The reason for this could be the heat transfer during grinding. In recent research projects, references were made to the high gradient in the residual stress depth curve caused by the high temperature development during grinding of hard materials [32–34]. This would also explain the abrupt drop of the high compressive residual stresses.

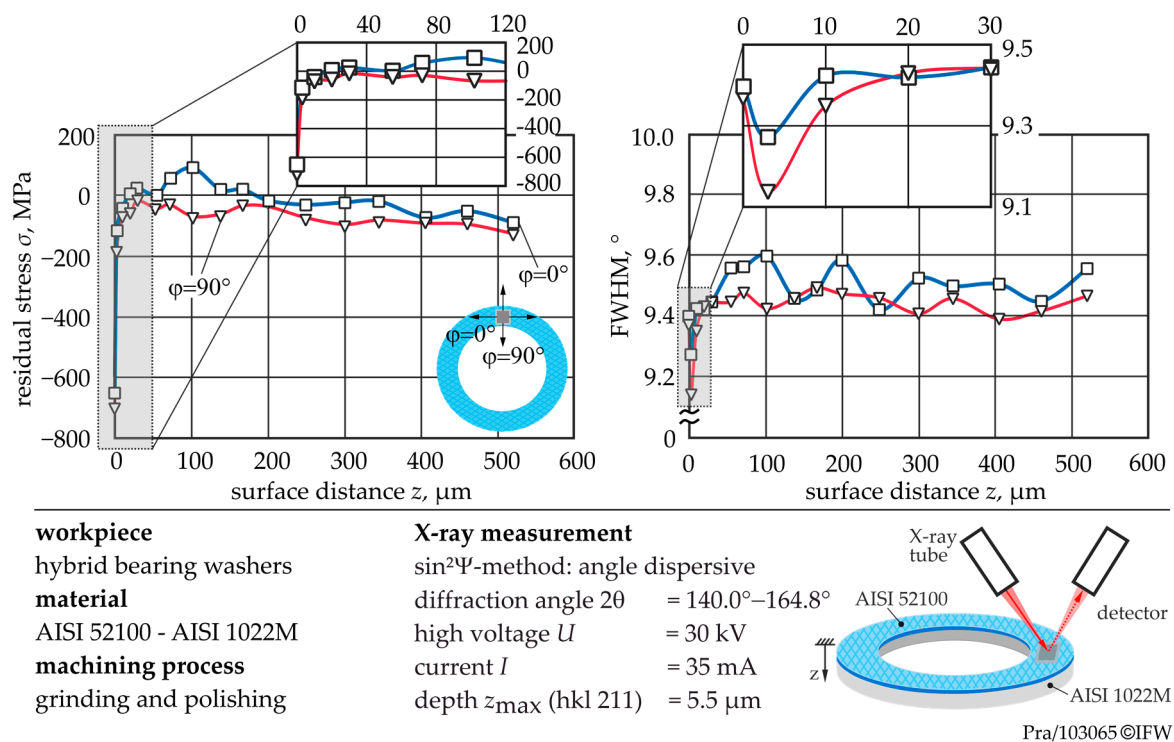


Figure 10. Residual stress and full width at half maximum (FWHM) depth profile after machining.

5.3. Microtribological Investigations

The coefficient of friction was calculated based on the performed scratch test for the cladding material. The microtribological investigations showed a coefficient of friction (CoF) of 0.4 for the considered hybrid bearing washer. This was in a good agreement to the CoF of industrial axial bearing made of AISI 52100, which was investigated in [14].

Figure 11 show the plastic behavior calculated by the nano-scratch tests. Without an additional forming and hardening of the axial bearing washer, a mean difference of 10.6 nm (standard deviation $SD = 2.46$) was achieved. The mean difference of the indentation depth with additional forming and hardening was about 9.5 nm ($SD = 2.55$), which corresponds to a decrease of about 11% between bearing washer with an additional forming step and without. However, the results of the industrial bearing washer made of AISI 52100 showed an even lower tendency to plastic deformation (8.6 nm with $SD = 3.13$) than the bearing washer made by means of the tailored forming process chain after the forming stage and a target heat treatment.

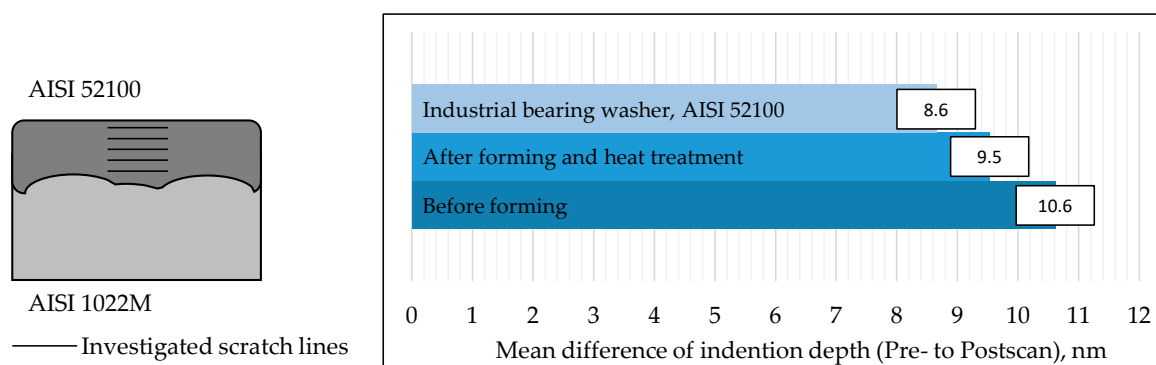


Figure 11. Evaluation of the scratch test of the cladding at different stages of the process chain.

These results indicate that the additional forming and heat treatment steps reduced the tendency to plastic deformation of the cladding material of the bearing washer made by the tailored forming process chain. However, industrially produced bearing washers have a lower tendency to plastic deformation than the hybrid bearing washer, so that individual process steps in the tailored forming process chain should be further optimized.

5.4. Optical and Acoustic Microscopy

Before fatigue testing, the washers were optically inspected. For the hybrid washers, the arithmetic mean value of the surface roughness R_a was measured as 95 ± 7 nm. The industrial standard is 80 nm. In applications with high speeds and high loads, bearing manufacturers usually recommend a mean roughness value of $R_a < 0.2$ μm for running surfaces in direct bearing arrangements, which was exceeded.

Via acoustic sectional images in axial direction (C-scan), various welding defects could be detected, as shown in Figure 12. At a depth between 150 and 300 μm from the surface, smaller pores are visible as white dots in the C-scan (circled in red in Figure 12a left). They have a typical size of 10–20 μm in diameter. The pores appeared randomly distributed. For the parameters investigated here with an axial load of 60 kN, the maximum of the Tresca equivalent stress is at a depth of approx. 125 μm . Since these pores occur in the zone of highest stress, they are rated as potentially critical. SAM images with higher magnification at this depth are shown in Figure 13 (bottom). The material transition zone between AISI 52100 and AISI 1022M lies in a depth of around 2.1 mm, which is shown in Figure 12a right. Here, larger cavities beyond 1 mm can be seen. These are arranged along the helical welding tracks (red arrows), which are about 10 mm apart. Concentric interference patterns are partially visible at the cavities, as there are repetitive echoes of the ultrasound signal. In order to support these findings, the sample was ground down layer by layer in the axial direction and compared to SAM imaging, see Figure 12b. The region of interest, marked in Figure 12a) on the right, is a 45° cutout. The cavities (circled in red in Figure 12b) open and close again in the course of 1.2 to 1.5 mm below the surface. Accordingly, the axial elongation is > 0.3 mm. By means of SAM (Figure 12a left), a greater degree of detail of the cavities is visible, as information was partially lost during the grinding process.

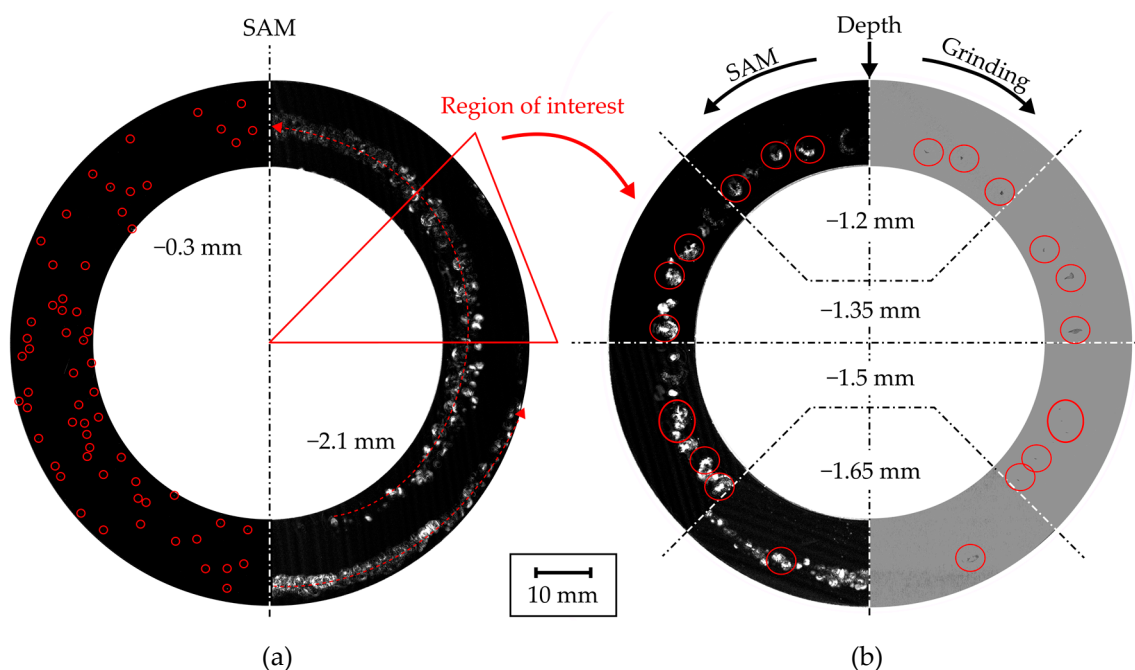


Figure 12. Scanning acoustic microscope images before testing: (a) Smaller pores near the surface (left) and larger cavities in the material transition zone (right); (b) comparison of scanning acoustic microscopy (SAM) (left) and optical microscopy after grinding (right) for different depths.

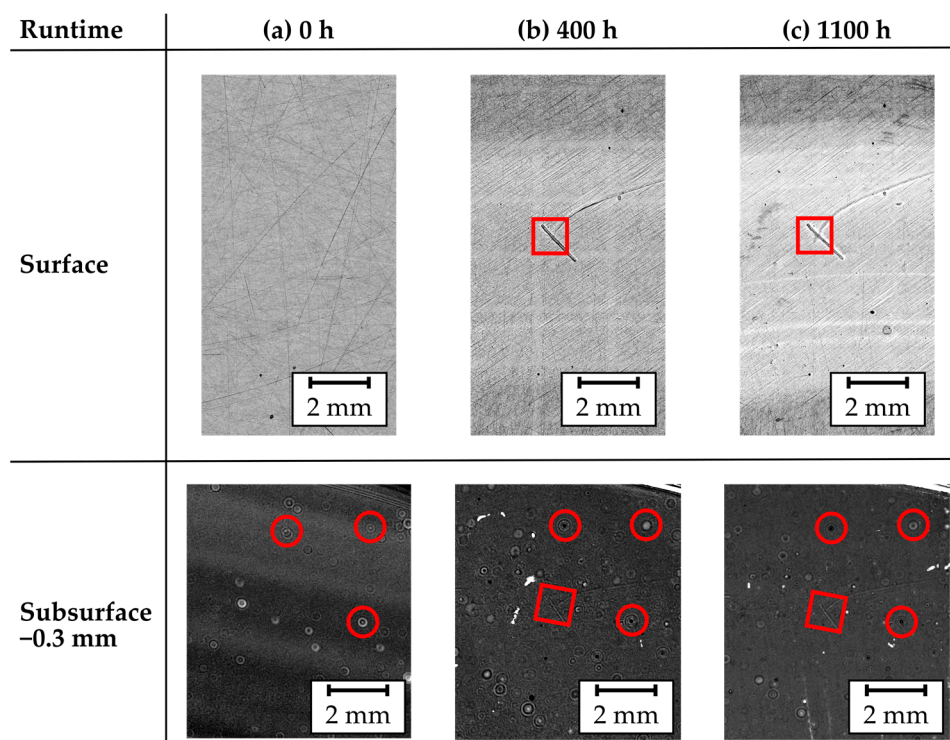


Figure 13. Optical (top) and acoustic (bottom) microscope images after: (a) machining; (b) 400 h runtime at 250 min^{-1} with surface damage; (c) test termination with 1100 h runtime at 250 min^{-1} .

5.5. Rolling Contact Fatigue Performance

5.5.1. Screening Test

First, a hybrid bearing washer with AISI 52100 cladding was tested on the FE8 test rig with 40 kN at 250 min^{-1} ($p_H = 1.85 \text{ GPa}$, $\kappa = 0.55$), in accordance with previous investigations [13,14]. In these investigations, maximum running times until failure of 260 h for a cladding with a martensitic chromium-silicon steel (AISI HNV3, 1.4718), and 332 h for a cladding with AISI 5140, were achieved.

The tailored forming washer with AISI 52100 cladding, on the other hand, ran 1100 h without a critical damage event. After this, the test was aborted and considered passed. The test was interrupted every 100 to 200 h to document the possible progression of the damage. The disc was extracted and examined visually, microscopically, and by means of SAM, see Figure 13. After 400 h, a surface defect with a maximum depth of $2.6 \mu\text{m}$ was detected.

The form of damage is unusual for damage that could have occurred during operation of the rolling bearing. It is more likely to be associated with a scrape mark during reassembly of the test. However, it is noticeable that this damage did not lead to the failure of the bearing. Even by means of ultrasonic microscopic images, no damage could be detected below the surface during continuous testing.

5.5.2. Pitting Tests

In order to shorten the test time, the test conditions were changed to the standardized test according to VW PV 1483 [35]. In the so-called pitting test, the axial load was 60 kN and was thus 50% higher than the previously mentioned conditions. This rolling bearing fatigue test usually aims to differentiate gear oils with regard to their pitting resistance. The test parameters are summarized in Table 4. The main criterion is a target running time of 200 h, divided into two phases:

1. Run-in procedure for 24 h at a reduced speed of 500 min^{-1} ,
2. Fatigue test for the remaining 176 h at 750 min^{-1} .

Table 4. Test conditions for fatigue testing of 81212 type tailored forming bearings.

| Parameter | | Value | Parameter | | Value |
|--------------------|------------|---------------------------|------------------|-----------|---------|
| Speed | n | 500–750 min^{-1} | Axial load | F_{ax} | 60 kN |
| Viscosity at 40 °C | ν_{40} | 68 mm^2/s | Load equivalent | C/P | 2.87 |
| Oil temperature | T_{Oil} | 95 °C | Contact load | F_1 | 3.16 kN |
| Viscosity ratio | k | 0.44 | Contact pressure | p_{max} | 1.8 GPa |

The fatigue life evaluation was carried out using Weibull analysis. Accordingly, the failure probability was calculated for $n = 6$ samples using maximum likelihood estimation and plotted in a double logarithmic diagram over the lifetime in Figure 14. A two-parameter Weibull distribution was assumed. The probability of error was 10%. The shape parameter, which indicates the slope of the regression line, was $\beta = 3.47$. The characteristic lifetime parameter indicated the lifetime at a failure probability of 63.2% and had a value of $B_{63} = 6.32 \times 10^6$ revolutions. The experimentally determined nominal life, which corresponds to a 10% probability of failure, is $B_{10} = 3.88 \times 10^6$ revolutions. This result serves as a baseline for future research with tailored forming bearings.

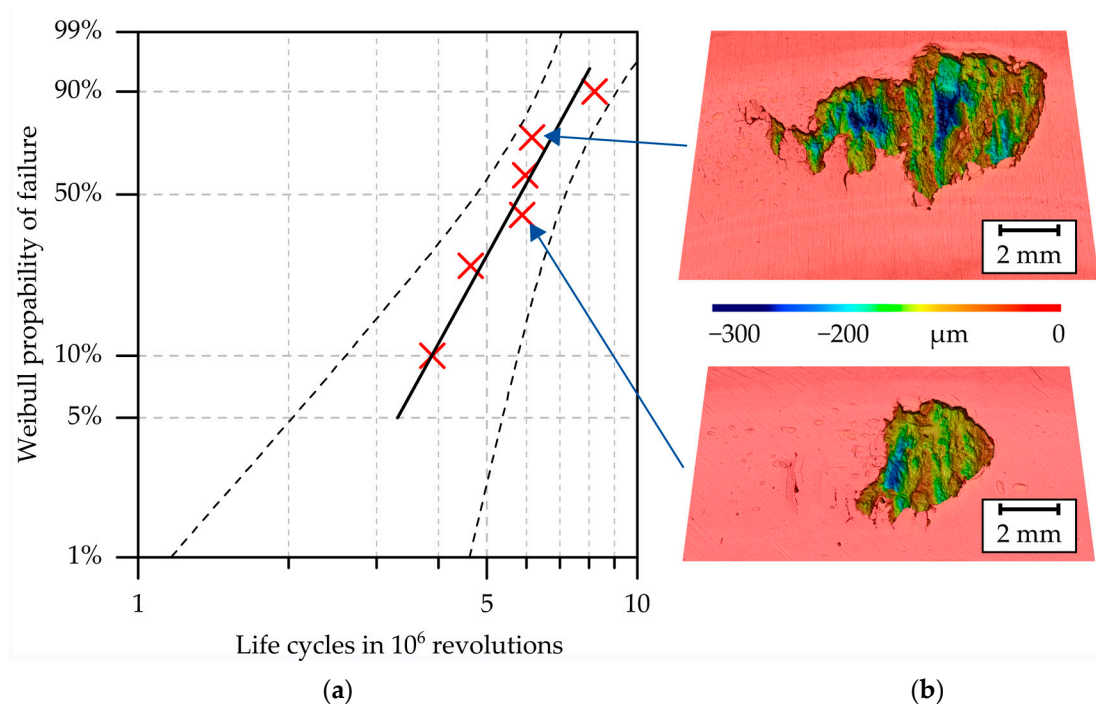


Figure 14. Bearing fatigue testing results: (a) Weibull plot with 95% confidence band for AISI 52100 tailored forming washers; (b) fatigue damage analysis by laser-scanning microscopy (rolling direction: right to left).

The theoretical rolling bearing life for conventional bearings can be calculated according to DIN ISO 281 [36], based on the work of Ioannides and Harris [37]. Since the operating speed of $500\text{--}750 \text{ min}^{-1}$ exceeds the thermally permissible speed, an adjusted reference speed of 300 min^{-1} was assumed for the lifetime calculation of conventional bearings as a reference. The additional factors are summarized in Table 5. The extended modified lifetime at a 90% survival probability was calculated to $L_{10m} = 4.75 \times 10^6$ revolutions. The deviation of the experimentally and mathematically determined lifetime is $B_{10}/L_{10m} = 81.68\%$. Thus, the bearing failures of AISI 52100 tailored forming bearings can be considered as premature failures due to small pores below the surface.

Table 5. Results of the fatigue life of tailored forming bearings and comparison with the calculated life of conventional bearings.

| Variable | | Value |
|-------------------------|-------------------------|--------------------------|
| Weibull shape parameter | β | 3.47 |
| Experimental life | B_{10} | 3.88×10^6 revs. |
| Adjusted speed | n_{ref} | 300 min^{-1} |
| Life exponent | p | 10/3 |
| Life factor | a_{ISO} | 0.14 |
| Modified rating life | $L_{10\text{m}}$ | 4.75×10^6 revs. |
| Deviation factor | $B_{10}/L_{10\text{m}}$ | 0.82 |

6. Conclusions

In this study, the tailored forming technology was successfully implemented for manufacturing of bearing components. Using plasma-transferred arc welding, classical bearing steel AISI 52100 was cladded on AISI 1022M basic steel and subsequently formed by upsetting. It served as cladding material for a rolling bearing raceway, which was investigated in bearing fatigue tests. The following conclusions can be drawn:

- AISI 52100 is considered as non-weldable, but it was possible to weld by means of PTA. The challenge of reducing pores during the welding process in order to increase the bearing fatigue life still remains.
- The forming process demonstrated a positive impact on the microstructure in the interface zone. Besides a grain refinement in the clad material, the Widmanstätten structure was fully recrystallized. Moreover, the porosity occurring after PTA was significantly reduced and a defect-free material transition between the base material and the cladding material was observed.
- Hardness values similar to those of industrial bearings were achieved by the applied heat treatment of quenching and tempering.
- Residual stress measurements demonstrated that no critical tensile residual stresses occurred at the surface of the hybrid bearing washers like in industrial bearing washers. High compressive residual stresses on the subsurface avoided premature failure of the bearing washers.
- By using AISI 52100 as cladding material, the load-bearing capacity of the tailored forming bearing washers was increased compared to AISI 5140 and AISI HNV3 claddings. Eighty-two percent of the calculated modified rating life for conventional bearings $L_{10\text{m}}$ was achieved. The slope of the determined Weibull curve indicates premature damage. By means of SAM, pores and cavities could be detected, which were probably responsible for this.

If the defects could be reduced or even completely prevented, a very high potential for improving the performance of tailored forming components opens up. In this context, follow-up investigations should consider in particular an optimization of the welding process by means of preheating and adapted welding materials as well as an increase in the degree of forming.

Author Contributions: Conceptualization, C.B., M.M., T.C.; investigation, C.B., F.S., M.Y.F., C.K., V.P., M.M., A.C., T.M., T.C.; writing—original draft preparation, C.B., F.S., M.Y.F., C.K., V.P., M.M., A.C., T.C.; writing—review and editing, F.P., F.N., T.H., B.B., L.B., J.H., B.-A.B., H.J.M., B.D., L.O., G.P.; visualization, C.B., F.S., M.Y.F., C.K., V.P., M.M., A.C., T.C.; supervision, F.P., F.N., T.H., B.B., B.-A.B., H.J.M., B.D., L.O., G.P. All authors have read and agreed to the published version of the manuscript.

Funding: This research was funded by the Deutsche Forschungsgemeinschaft (DFG, German Research Foundation) under grant number 252662854.

Acknowledgments: The results presented in this paper were obtained within the Collaborative Research Centre 1153 “Process chain to produce hybrid high performance components by Tailored forming”—252662854—in the subprojects A2, A4, B2, B4, C1, and C3. The authors thank the German Research Foundation (DFG) for their financial support of this project.

Conflicts of Interest: The authors declare no conflict of interest.

References

1. Blohm, T.; Mildebrath, M.; Stonis, M.; Langner, J.; Hassel, T.; Behrens, B.-A. Investigation of the cladding thickness of plasma-transferred arc deposition welded and cross wedge rolled hybrid parts. *Prod. Eng.* **2017**, *11*, 255–263. [\[CrossRef\]](#)
2. Mildebrath, M.; Blohm, T.; Hassel, T.; Stonis, M.; Langner, J.; Maier, H.J.; Behrens, B.-A. Influence of Cross Wedge Rolling on the Cladding Quality of Plasma-Transferred Arc Deposition Welded Hybrid Steel Parts. *Int. J. Emerg. Technol. Adv. Eng.* **2017**, *7*, 1–7.
3. Cento, P.; Dareing, D.W. Ceramic Materials in Hybrid Ball Bearings. *Tribol. Trans.* **1999**, *42*, 707–714. [\[CrossRef\]](#)
4. Wan, G.T.Y.; Gabelli, A.; Ioannides, E. Increased Performance of Hybrid Bearings with Silicon Nitride Balls. *Tribol. Trans.* **1997**, *40*, 701–707. [\[CrossRef\]](#)
5. Dill, J.F. Hybrid bearing technology for advanced turbomachinery. *J. Eng. Gas Turbines Power* **1996**, *118*, 173–178. [\[CrossRef\]](#)
6. Koehler, H.; Schumacher, J.; Schuischel, K.; Partes, K.; Bomas, H.; Jablonski, F.; Vollertsen, F.; Kienzler, R. An approach to calculate fatigue properties of laser clad components. *Prod. Eng.* **2012**, *6*, 137–148. [\[CrossRef\]](#)
7. Koehler, H.; Partes, K.; Seefeld, T.; Vollertsen, F. Influence of laser reconditioning on fatigue properties of crankshafts. *Phys. Procedia* **2011**, *12*, 512–518. [\[CrossRef\]](#)
8. Alam, M.M.; Kaplan, A.; Tuominen, J.; Vuoristo, P.; Miettinen, J.; Poutala, J.; Näkki, J.; Junkala, J.; Peltola, T.; Barsoum, Z. Analysis of the stress raising action of flaws in laser clad deposits. *Mater. Des.* **2013**, *46*, 328–337. [\[CrossRef\]](#)
9. Chew, Y.; Hock Lye Pang, J.; Bi, G.; Song, B. Effects of laser cladding on fatigue performance of AISI 4340 steel in the as-clad and machine treated conditions. *J. Mater.* **2017**, *243*, 246–257. [\[CrossRef\]](#)
10. Pape, F.; Coors, T.; Poll, G. Studies on the Influence of Residual Stresses on the Fatigue Life of Rolling Bearings in Dependence on the Production Processes. *Front. Mech. Eng.* **2020**, *6*. [\[CrossRef\]](#)
11. Mildebrath, M.; Coors, T.; Barroi, A.; Pape, F.; Lammers, M.; Hermsdorf, J.; Overmeyer, L.; Poll, G.; Hassel, T. Herstellungsprozess und Wälzfestigkeit von hybriden Hochleistungsbauteilen. *Konstruktion* **2018**, *9*, 84–89.
12. Behrens, B.-A.; Amiri, A.; Duran, D.; Nothdurf, S.; Hermsdorf, J.; Kaierle, S.; Ohrdes, H.; Wallaschek, J.; Hassel, T. Improving the mechanical properties of laser beam welded hybrid workpieces by deformation processing. *AIP Conf. Proc.* **2019**, *2113*. [\[CrossRef\]](#)
13. Pape, F.; Coors, T.; Barroi, A.; Hermsdorf, J.; Mildebrath, M.; Hassel, T.; Kaierle, S.; Matthias, T.; Chugreev, A.; Chugreeva, A.; et al. Tribological Study on Tailored-Formed Axial Bearing Washers. *Tribol. Online* **2018**, *12*. [\[CrossRef\]](#)
14. Behrens, B.-A.; Chugreev, A.; Matthias, T.; Poll, G.; Pape, F.; Coors, T.; Hassel, T.; Maier, H.J.; Mildebrath, M. Manufacturing and Evaluation of Multi-Material Axial-Bearing Washers by Tailored forming. *Metals* **2019**, *9*, 232. [\[CrossRef\]](#)
15. Stanford, M.K.; Jain, V.K. Friction and wear characteristics of hard cladding. *Wear* **2001**, *251*, 990–996. [\[CrossRef\]](#)
16. Matthes, K.; Schneider, W. *Schweißtechnik—Schweißen von metallischen Konstruktionswerkstoffen*, 6th ed.; Hanser Verlag: München, Germany, 2016; pp. 33–34.
17. Schneider, W.; Twarddek, J. *Praxiswissen Schweißtechnik*, 6th ed.; Springer: Wiesbaden, Germany, 2019; p. 268.
18. Diltthey, U. *Schweißtechnische Fertigungsverfahren 2—Verhalten der Werkstoffe beim Schweißen*, 3rd ed.; Springer: Berlin, Germany, 2005; p. 130.
19. Kittner, K.; Wiesner, J.; Kawalla, R. A new approach for void closure in bulk metal forming. *Key Eng. Mater.* **2016**, *716*, 595–604. [\[CrossRef\]](#)
20. DIN EN ISO 6507, *Metallic Materials—Vickers Hardness Test*; International Organization for Standardization: Geneva, Switzerland, 2005.
21. DIN EN ISO 6508, *Metallic Materials—Rockwell Hardness Test*; International Organization for Standardization: Geneva, Switzerland, 2005.
22. Krektuleva, R.V.; Cherepanov, O.I.; Cherepanov, R.O. Numerical investigation of residual thermal stresses in welded joints of heterogeneous steels with account of technological features of multi-pass welding. *Appl. Math. Model.* **2016**, *42*, 244–256. [\[CrossRef\]](#)

23. Kanakaraju, V.; Gunjal, S.; Rathinam, K.; Sharma, P. Optimization of cutting parameters of residual stresses in simultaneous turning technique. *Mater. Today Proc.* **2020**, *28*, 2108–2115. [[CrossRef](#)]
24. Jawahir, I.S.; Brinksmeier, E.; M'Saoubi, R.; Aspinwall, D.K.; Outeiro, J.C.; Meyer, D.; Umbrello, D.; Jayal, A.D. Surface integrity in material removal processes: Recent advances. *CIRP Ann.* **2011**, *60*, 603–626. [[CrossRef](#)]
25. Breidenstein, B. Oberflächen und Randzonen hoch Belasteter Bauteile. Habilitation Thesis, Leibniz University Hannover, Hannover, Germany, 2011.
26. Novovic, D.; Dewes, R.C.; Aspinwall, D.K.; Voice, W.; Bowen, P. The effect of machined topography and integrity on fatigue life. *Int. J. Mach. Tools Manuf.* **2004**, *44*, 125–134. [[CrossRef](#)]
27. Guo, J.; Fu, H.; Pan, B.; Kang, R. Recent progress of residual stress measurement methods: A review. *Chin. J. Aeronaut.* **2020**. [[CrossRef](#)]
28. Macherauch, E.; Müller, P. Das sin2psi-Verfahren der röntgenographischen Spannungsmessung. *Z. Angew. Phys.* **1961**, *13*, 305–312.
29. Eigenmann, B.; Macherauch, E. Röntgenographische Untersuchung von Spannungszuständen in Werkstoffen, Teil III. *Mater. Werkst.* **1996**, *27*, 426–437. [[CrossRef](#)]
30. DIN 51819, *Testing of Lubricants—Mechanical-Dynamic Testing in the Roller Bearing Test Apparatus FE8—Part 1: General working principles*; Deutsches Institut für Normung e.V.: Berlin, Germany, 2016.
31. ISO 16889, *Hydraulic Fluid Power—Filters—Multi-Pass Method for Evaluating Filtration Performance of a Filter Element*; International Organization for Standardization: Geneva, Switzerland, 2008.
32. Jamshidi, H.; Budak, E. Grinding Temperature Modeling Based on a Time Dependent Heat Source. *Procedia CIRP* **2018**, *77*, 299–302. [[CrossRef](#)]
33. Zhao, Z.; Qian, N.; Ding, W.; Wang, Y.; Fu, Y. Profile grinding of DZ125 nickel-based superalloy: Grinding heat, temperature field, and surface quality. *J. Manuf. Process.* **2020**, *57*, 10–22. [[CrossRef](#)]
34. Rabiey, M.; Maerchy, P. Investigation on Surface Integrity of Steel DIN 100Cr6 by Grinding Using CBN Tool. *Procedia CIRP CSI* **2020**, *87*, 192–197. [[CrossRef](#)]
35. VW PV 1483, *Factory Standard, Gear Oils—Testing the Pitting Load Capacity in Rolling Bearings (in German)*; Volkswagen AG: Wolfsburg, Germany, 2007.
36. DIN ISO 281, *Rolling Bearings—Dynamic Load Ratings and Rating Life*; International Organization for Standardization: Geneva, Switzerland, 2007.
37. Ioannides, E.; Bergling, G.; Gabelli, A. An Analytical Formulation for the Life of Rolling Bearings. In *Acta Polytechnica Scandinavica*; Mechanical Engineering Series 137; Finnish Academies of Technology: Espoo, Finland, 1999.



© 2020 by the authors. Licensee MDPI, Basel, Switzerland. This article is an open access article distributed under the terms and conditions of the Creative Commons Attribution (CC BY) license (<http://creativecommons.org/licenses/by/4.0/>).